CrossMark

ORIGINAL PAPER

Anisotropy of self-diffusion in forsterite grain boundaries derived from molecular dynamics simulations

Johannes Wagner[1] · Omar Adjaoud[2] · Katharina Marquardt[3] · Sandro Jahn[1,4]

Abstract Diffusion rates and associated deformation behaviour in olivine have been subjected to many studies, due to the major abundance of this mineral group in the Earth's upper mantle. However, grain boundary (GB) transport studies yield controversial results. The relation between transport rate, energy, and geometry of individual GBs is the key to understand transport in aggregates with lattice preferred orientation that favours the presence and/or alignment of specific GBs over random ones in an undeformed rock. In this contribution, we perform classical molecular dynamics simulations of a series of symmetric and one asymmetric tilt GBs of Mg_2SiO_4 forsterite, ranging from 9.58° to 90° in misorientation and varying surface termination. Our emphasis lies on unravelling structural characteristics of high- and low-angle grain boundaries and how the atomic structure influences grain boundary excess volume and self-diffusion processes. To obtain diffusion rates for different GB geometries, we equilibrate the respective systems at ambient pressure and temperatures from 1900 to 2200 K and trace their evolution for run durations of at least 1000 ps. We then calculate the mean square displacement of the different atomic species within the GB interface to estimate self-diffusion coefficients in the individual systems. Grain boundary diffusion coefficients for Mg, Si and O range from 10^{-18} to 10^{-21} m^3/s, falling in line with extrapolations from lower temperature experimental data. Our data indicate that higher GB excess volumes enable faster diffusion within the GB. Finally, we discuss two types of transport mechanisms that may be distinguished in low- and high-angle GBs.

Keywords Forsterite · Grain boundary · Self-diffusion · Mg

Introduction

Grain boundaries (GBs) in oxides and silicates have received increased attention in the last decades, as they are known to influence many key physical and chemical properties of rocks (Dohmen and Milke 2010) such as reaction kinetics (Keller et al. 2008), fluid transport (Gardés et al. 2012), chemical alteration (Hartmann et al. 2008), electrical conductivity (Pommier et al. 2015), and solid-state diffusion (Marquardt et al. 2011). GBs in the mineral group olivine, $(Mg,Fe)_2SiO_4$, have been studied extensively to elucidate their role in the rheological behaviour of the upper mantle. The ongoing debate whether dislocation or diffusion creep dominates the plastic deformation of the mantle and where transitions between the two may occur (Karato and Wu 1993; Hansen et al. 2012; Hirth and Kohlstedt 2013) has led to extensive research of the bulk self-diffusion kinetics of olivine (e.g. Chakraborty et al. 1994; Dohmen et al. 2002, 2007; Fei et al. 2012, 2013) and its polymorphs (Farber et al. 1994; Shimojuku et al. 2004; Kubo et al. 2004; Shimojuku et al. 2009). However, in the

✉ Sandro Jahn
 s.jahn@uni-koeln.de

1 GFZ German Research Centre for Geosciences, Telegrafenberg, 14473 Potsdam, Germany

2 Institute of Materials Science, Technische Universität Darmstadt, 64287 Darmstadt, Germany

3 Bayerisches Geoinstitut, BGI, University of Bayreuth, Universitätsstrasse 30, 95447 Bayreuth, Germany

4 Institute of Geology and Mineralogy, University of Cologne, Zülpicher Strasse 49b, 50674 Köln, Germany

case of grain boundary diffusion in olivine, experimental data are limited. Diffusion measurements in forsterite GBs have been reported by Farver et al. (1994) for magnesium, Farver and Yund (2000) and Fei et al. (2016) for silicon, and Condit et al. (1985) for oxygen.

Another approach that has been much less utilised so far is to look at (grain boundary) diffusion from a molecular simulation perspective. Such simulations enable us not only to calculate physical and thermodynamic properties of a given system (total energy, electrical conductivity, chemical diffusion) but simultaneously link them to structural properties on a molecular scale. Ammann et al. (2010) reviewed static first principles simulations to calculate bulk diffusion rates in perovskite and periclase. In such static studies, the frequency of atom jumps to vacant lattice sites is derived from the lowest energy barrier that has to be crossed and the frequency of attempts derived from harmonic transition-state theory. Ghosh and Karki (2013) investigated the energetics and structure of a set of Mg_2SiO_4 forsterite tilt grain boundaries using similar methods and infer that, depending on misorientation, areas of low density in these GBs may serve as fast diffusion pathways. An alternative approach is to perform molecular dynamics (MD) simulations where atomic displacements are followed in real time by integration of Newton's equations of motion. Subsequently, the systems evolution is tracked over time in order to average over a property of interest. However, simulations based on first principles are computationally expensive and typically limited to the simulation of a few hundred atoms and picoseconds of simulation time. In the case of GBs, simulation cells need to be sufficiently large to exclude finite size effects (e.g. interaction of repeated GBs introduced by the periodic boundary conditions) and to capture the entire repeat unit length along a GB. To investigate self-diffusion directly by molecular dynamics simulations, simulation times have to be sufficiently long to generate statistically meaningful displacements of atoms that may be considered as diffusing. One possible solution to these obstacles is to perform MD simulations based not on first principles but on classical interaction potentials. Such simulations have the advantage that they are computationally much less expensive and thus enable the simulation of comparatively large systems (several 1000 atoms) and long timescales (several nanoseconds). Nevertheless, classical MD still requires comparatively high temperatures to reach a sufficient degree of atomic mobility in order to catch diffusive processes at all. In this study, we estimate major element grain boundary self-diffusion coefficients in a set of Mg_2SiO_4 forsterite tilt grain boundaries using classical MD simulations. We utilise an advanced ionic interaction potential that has been successfully applied in the simulation of many oxides and silicates, including forsterite (e.g. Jahn and Madden 2007; Adjaoud et al. 2012; Finkelstein et al. 2014).

Simulation procedure

Grain boundary set-up

We constructed several Mg_2SiO_4 forsterite (space group *Pbnm*, $a = 4.7535$ Å, $b = 10.1943$ Å, $c = 5.9807$ Å $\alpha = \beta = \gamma = 90°$) grain boundaries with misorientation angles varying from 9.58° to 90°. Details about the procedure, grain boundary energies, and structure of all (0kl)/[100] symmetric tilt grain boundaries are reported in Adjaoud et al. (2012). Briefly, grain boundaries are generated by cutting a crystal grain at a specific angle and then one-half of the crystal grain is rotated by 180° with respect to the other half. The rotation axis is perpendicular to the cutting plane. Leaving a small gap between the two grains, one grain is systematically shifted with respect to the other grain in the interface plane. This procedure allows to create several atomic configurations for each misorientation angle. The total energy of each atomic configuration is calculated. The atomic configurations with the lowest energy are subsequently relaxed by MD at ambient conditions, which leads to the closure of the gap and the construction of a structural model for the specific symmetric tilt grain boundary. Additionally, as they are among the most abundant GBs in undeformed forsterite aggregates (Marquardt et al. 2015), a 90° misorientation grain boundary containing 9744 atoms is constructed in a similar manner for this study, bringing in contact two forsterite grains with (100) and (010) free surfaces. The new cell containing the 90° misorientation grain boundary has the cell dimensions $32.98 \times 38.43 \times 12.93$ Å and is also annealed at ambient conditions. The termination of the (100) and (010) surfaces is chosen as to represent the lowest energy termination according to Watson et al. (1997).

Self-diffusion coefficients from MD simulations

Next, we use classical MD simulations to study the structure and transport mechanisms of the constructed grain boundaries at high temperatures. First, we equilibrate each system at ambient pressure and temperatures between 1900 and 2200 K (*NPT* ensemble, constant number of particles N, constant pressure P, constant temperature T) for at least 2 ps. Given the nanosecond timescale available to our simulations, such comparatively high temperatures are necessary to reach a sufficient degree of atomic mobility. Temperature and pressure are controlled by a Nosé–Hoover thermostat (Nosé and Klein 1983) coupled to a barostat (Martyna et al. 1994). We subsequently fix the cell volume V and track the system evolution at a given temperature for at least 1000 ps with 1 fs timesteps (*NVT* ensemble using a Nosé–Hoover thermostat to control the temperature). System sizes range from 4032 to 9744 atoms, periodic

boundary conditions are applied in every simulation. The movement of individual elements is evaluated by analysing their mean squared displacements (MSD) over the duration of the simulation. It is assumed that, in terms of diffusion, a steady state is reached as soon as the MSD increases linearly with time, which is the case for all simulations in this study. Self-diffusion coefficients can then be estimated using Einstein's relation between self-diffusion coefficient and MSD (Allen and Tildesley 1989):

$$D_i = \lim_{t \to \infty} \frac{\left\langle (\boldsymbol{r}(t + t_0) - \boldsymbol{r}(t_0))^2 \right\rangle}{2 \cdot \dim \cdot t} \tag{1}$$

where D_i is the self-diffusion coefficient of element i (Mg, Si, O). $\boldsymbol{r}(t)$ is the position vector of an individual atom of type i at time t and dim the dimensionality of the system. The numerator at the right-hand side of Eq. 1 is the mean squared displacement, which is averaged over all atoms N_i of a specific element i starting with an initial time t_0 (symbolised by angular brackets). Conventionally, Eq. 1 is defined for systems where all atoms of a specific element contribute to a homogeneous self-diffusion coefficient (e.g. a fluid). However, in the case of grain boundaries, self-diffusion within the bulk crystal can be several orders of magnitude slower as compared to the GB (e.g. Farver and Yund 2000; Dohmen and Milke 2010; Marquardt et al. 2011). As a consequence, a MSD that averages over all the atoms of a specific element in these systems also averages over the comparatively immobile atoms within the bulk crystal. This leads to a considerable underestimation of the grain boundary diffusion, and it is thus compulsory to treat the GB and the bulk crystal as two sub-systems (e.g. Fisler and Mackwell 1994). Therefore, we analyse the distribution of the MSDs of each individual atom and only consider those that have been displaced more than 7 Å² at a time interval of at least 1000 ps and hence contribute significantly to GB diffusion. Choosing a slightly lower or higher cut-off (e.g. 6 Å² or 8 Å²) does not change the MSD results significantly. However, a too low cut-off will average over atoms that have not moved beyond their nearest neighbour distance, while a higher cut-off will ignore atoms that have been diffusing only short distances in the MD timescale. We chose 7 Å² as a compromise and kept the cut-off for all calculations. To gain further insight into the influence of grain boundary geometry and stability on the self-diffusion coefficient, we also calculate the excess volume (V^{Gb}) of each individual GB as follows:

$$V^{Gb} = \frac{V^{bc} - V^{sc}}{2A^{Gb}} \tag{2}$$

where V^{bc} and V^{sc} are the total volumes of the grain boundary cell and a reference single crystal, respectively. A^{Gb} is the area of the grain boundary and the factor 2 accounts for the fact that the actual simulation cell contains two grain boundaries due to the periodic boundary conditions.

Classical interaction potential

All simulations are performed using a set of classical interaction potentials parametrised for the Ca–Mg–Al–Si–O system by reference to first principles electronic structure calculations (Jahn and Madden 2007). In addition to charge–charge (i.e. Coulomb) interactions and dispersion, this model includes true many-body effects by accounting for polarisation effects (electronic multipoles up to quadrupoles) as well as aspherical shape deformation of anions, depending on their local environment (Madden et al. 2006). Multipoles and shape deformations are computed self-consistently at each simulation step. Such aspherical ion model (AIM) potentials have been successfully applied in the simulation of several geomaterials including forsterite (Jahn and Madden 2007; Jahn and Martoňák 2008; Jahn 2010), oxide and silicate melts and interfaces (Adjaoud et al. 2008, 2011; Jahn and Madden 2008; Gurmani et al. 2011) as well as forsterite grain boundaries (Adjaoud et al. 2012). All simulations in this contribution are performed using the CP2K code package (Hutter et al. 2014) with an implementation of the AIM potential type made recently by the authors. All potential parameters are listed in Jahn and Madden (2007).

Results

Grain boundary self-diffusion coefficients D_i derived from Eq. 1 and averaged over the mobile ions only are given in Table 1. For silicon and occasionally oxygen, self-diffusion rates are very low (in the order of 10^{-12} m²/s and below) and only few atoms move beyond the MSD cut-off of 7 Å² within the simulation time frame. In some cases, it is impossible to extract meaningful self-diffusion coefficients and the respective entries in the data set are thus left blank. To make our results comparable to experimental diffusion data, we also present the grain boundary diffusion coefficients from the simulations as the product of D_i and the effective grain boundary width δ, which is set to 10^{-9} m (Ricoult and Kohlstedt 1983). The resulting δD_i^{Gb} is normalised to the total number of ions i (including immobile ions) in the grain boundary interface volume, which is defined by δ times the grain boundary area. The respective δD_i^{Gb} are presented in Table 1. Experimental data for the temperature range of our simulations are not available. However, Figs. 1, 2, and 3 compare our results to linear extrapolations of various experimental studies in lower temperature regimes. The figures also contain self-diffusion coefficients of Mg_2SiO_4 melt derived by Adjaoud

et al. (2008) using the same MD model. Grain boundary excess volumes V^{Gb} calculated according to Eq. 2 are given in Table 1.

Discussion

Self-diffusion coefficients

Overall, data derived directly from our MD simulations are well in the range of extrapolations from lower temperature experimental data. In the case of Mg, the δD_{Mg}^{Gb} from the simulation plot somewhat below the extrapolated line from the experiments, which may have various reasons. In addition to possible systematic errors of the simulations due to the chosen interaction potential, the spread of the experimental data leads to a relatively large uncertainty for extrapolations to much higher temperatures. Close to the melting point of forsterite, the activation energy for grain boundary diffusion may become smaller and eventually approach the self-diffusion coefficient of the melt, which is in the order of 10^{-18} m³/s for Mg (Adjaoud et al. 2008, 2011). Finally, the δD_{Mg}^{Gb} may be underestimated as ions having moved less than the cut-off distance are considered immobile, whereas in real samples slowly moving ions also contribute to δD_{Mg}^{Gb}.

In the case of Si, the few data that can be extracted from our simulations plot between the linear regression of the data sets of Farver and Yund (2000) and Fei et al. (2016). Oxygen self-diffusion coefficients predicted by our simulations are well in line with data by Condit et al. (1985) and seem to be systematically smaller than data from Fisler and Mackwell (1994). The low δD_O^{Gb} predicted by our simulations may also be due to the used AIM potential, which is known to generally predict too strong oxygen bonds and may lead to a reduced oxygen mobility (Adjaoud et al. 2008). The experimental results of Watson (1986) appear to be several orders of magnitude to high, as they surpass self-diffusion coefficients predicted even for a Mg_2SiO_4 liquid already at low temperatures. The large spread of experimental oxygen diffusion data ranging from 10^{-16} to 10^{-24} m³/s for temperatures between 1200 and 1500 K make a robust assessment of the simulation data difficult. The discrepancies in experimental data sets may be due to the various methodologies employed in the experiments, comprising isotopic tracer analysis (Condit et al. 1985; Farver and Yund 2000; Fei et al. 2016) and indicator mineral reactions (Watson 1986; Fisler and Mackwell 1994).

Consequently, the MD results are not necessarily comparable to a specific set of experiments, as the diffusion mechanisms involved may be different in the high- and low-temperature regimes. At the highest MD temperatures,

Table 1 MD simulation results for all investigated grain boundaries

GB angle (°)	T (K)	D_{Mg}	δD_{Mg}^{Gb}	D_{Si}	δD_{Si}^{Gb}	D_O	δD_O^{Gb}	V^{Gb} (Å³/Å²)
9.58	2200	8.34	12.7	–	–	–	–	0.66
11.17	2200	10.3	17.4	–	–	2.61	2.67	0.72
16.69	2200	9.93	25.0	5.77	0.59	2.14	2.14	0.80
32.7	2200	9.98	26.8	–	–	–	–	0.94
	2100	4.82	10.8	–	–	1.02	1.01	1.00
	1900	2.23	0.93	–	–	1.08	0.18	0.92
60.8[a]	2200	3.42	5.15	–	–	–	–	0.34
60.8	2200	4.14	6.23	–	–	1.30	0.89	0.55
	2100	2.90	2.62	–	–	1.04	0.53	0.51
	1900	1.34	0.44	–	–	0.44	0.14	0.52
90.0	2200	32.9	136.0	7.75	9.93	7.11	16.4	1.30
	2100	25.5	84.1	3.31	23.4	4.97	7.94	1.20
	2000	13.6	29.9	1.64	0.54	–	–	1.19
	1900	8.30	12.8	–	–	3.23	2.22	1.18

For Mg, Si, and O, two data sets are given: (1) the self-diffusion coefficients D_i, derived from MSD after 1000 ps run duration, averaging over all atoms moving beyond the 7 Å² cut-off (given in 10^{-11} m²/s). (2) The same self-diffusion coefficient normalised to the grain boundary volume, denoted as δD_i^{Gb} (given in 10^{-20} m³/s with $\delta = 1$ nm). Additionally, the excess volume for every configuration is given (see text). Gaps in the data set occur when diffusion was too slow to be statistically captured on the timescale of the MD simulation
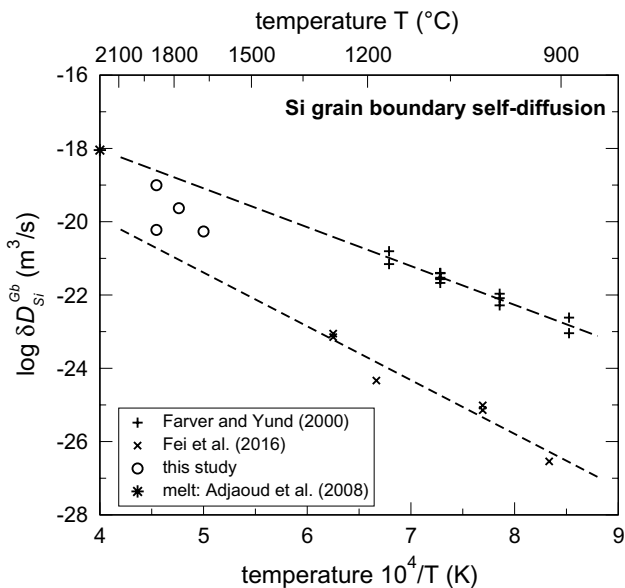
[a] Asymmetrical
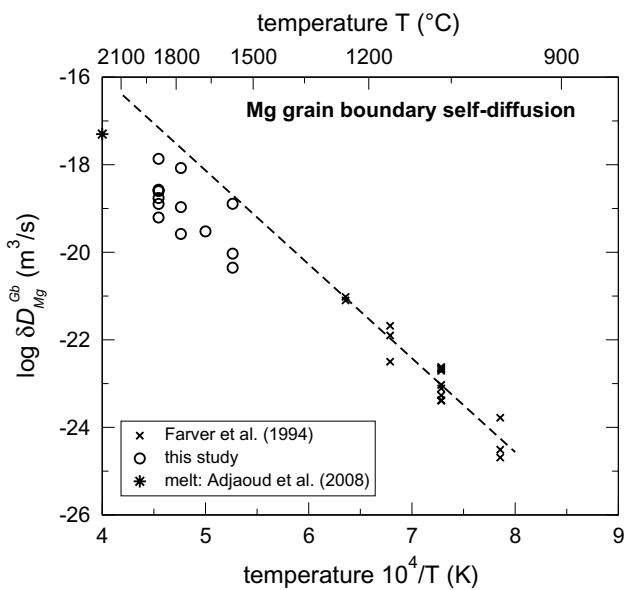
Fig. 1 Mg grain boundary diffusion coefficients from MD simulations (this study) compared to experimental data (Farver et al. 1994) and to the Mg self-diffusion coefficient in Mg_2SiO_4 melt from MD simulations of Adjaoud et al. (2008). The *dashed line* is a linear extrapolation of data by Farver et al. (1994)
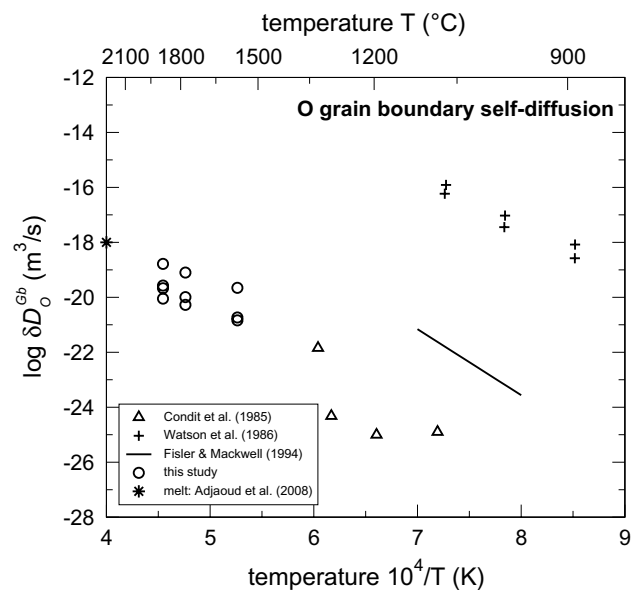
Fig. 3 Oxygen grain boundary diffusion coefficients from MD simulations (this study) compared to experimental data (Condit et al. 1985; Watson 1986; Fisler and Mackwell 1994) and to the oxygen self-diffusion coefficient in Mg_2SiO_4 melt from MD simulations of Adjaoud et al. (2008)

Fig. 2 Si grain boundary diffusion coefficients from MD simulations (this study) compared to experimental data (Farver and Yund 2000; Fei et al. 2016) and to the Si self-diffusion coefficient in Mg_2SiO_4 melt from MD simulations of Adjaoud et al. (2008). The *dashed lines* are linear extrapolations of data by Farver and Yund (2000) and Fei et al. (2016)

atoms may diffuse rather liquid-like in the grain boundary zone, while at experimental temperatures, energy barriers are much higher and mechanisms such as vacancy

migration play a stronger role. Moreover, our simulations represent ideal systems as opposed to experimental systems where impurities will influence diffusion. This means that we by no means wish to support or refute a specific set of experiments, but rather emphasise that the data predicted by the MD approach are reasonable and justify the discussion below.

Grain boundary transport mechanisms and volume dependence

To visualise the molecular-scale transport mechanism in different GB types, Figs. 4 and 5 show exemplary snapshots of the MD trajectories for a low-angle (9.58°) and a high-angle grain boundary (60.8°). The upper panels (A) in both figures show the overall displacement of individual atoms at the last snapshot of the respective simulation. It is readily visible in both examples that the repeated grain boundaries, which result from the periodic boundary conditions, are well separated and do not interact. Low-angle GBs in general can be described as an array of aligned partial dislocations and stacking faults (e.g. Ikuhara et al. 2003, in alumina). In Fig. 4, it is readily visible that diffusion takes place in a confined space around these partial dislocations in the bicrystal lattice (see Adjaoud et al. (2012) for a detailed analysis of the structures presented). These areas of highest mobility are likely correlated to the spatial extend of the dislocation cores, have radii of

Fig. 4 a Snapshot of the trajectory of a low-angle grain boundary (9.58° misorientation) with individual atoms coloured according to their overall displacement with respect to the first step of the run. The *black dashed lines* indicate the misorientation angle. **b**, **c** show exemplary trajectories of Mg atoms propagating through the diffusion channel (see text). The *green dashed line* indicates the extend of one of these channels. Different trajectory colours are individual atoms. The cell in the centre image is rotated about 2° around the *z*-axis. All figures are created using the OVITO software (Stukowski 2010)
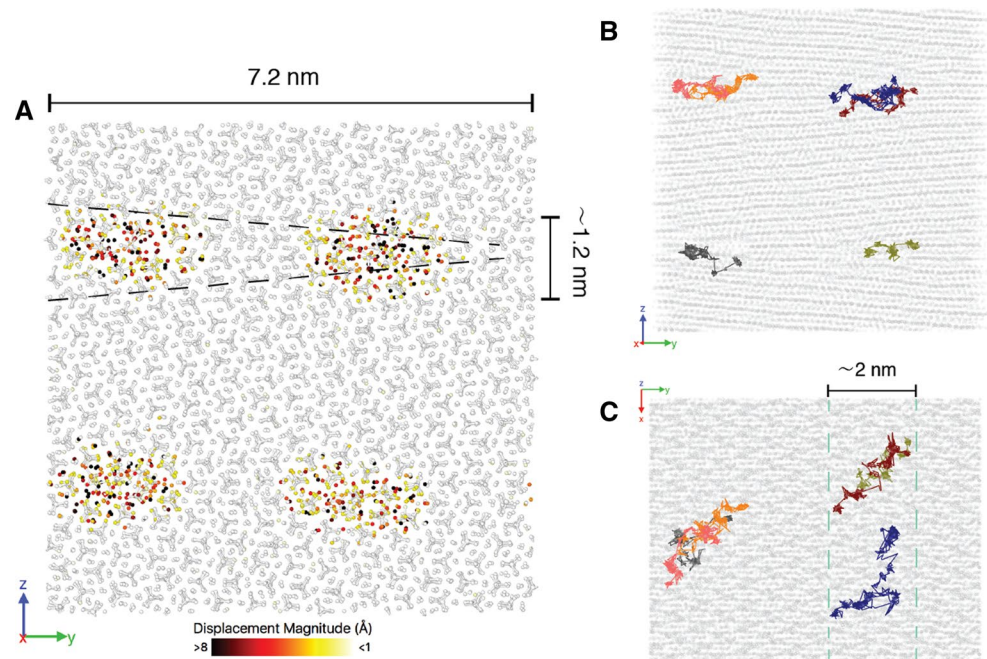

Fig. 5 a Snapshot of the trajectory of a high-angle grain boundary (60.8° misorientation) with individual atoms coloured according to their overall displacement with respect to the first step of the run. The *black dashed lines* indicate the misorientation angle. **b**, **c** show exemplary trajectories of Mg atoms propagating through the diffusive layer (outlined in *green*) of the GB interface (see text). Different trajectory colours are individual atoms. The cell in the centre image is rotated about 20° around the *z*-axis. All figures are created using the OVITO software (Stukowski 2010)
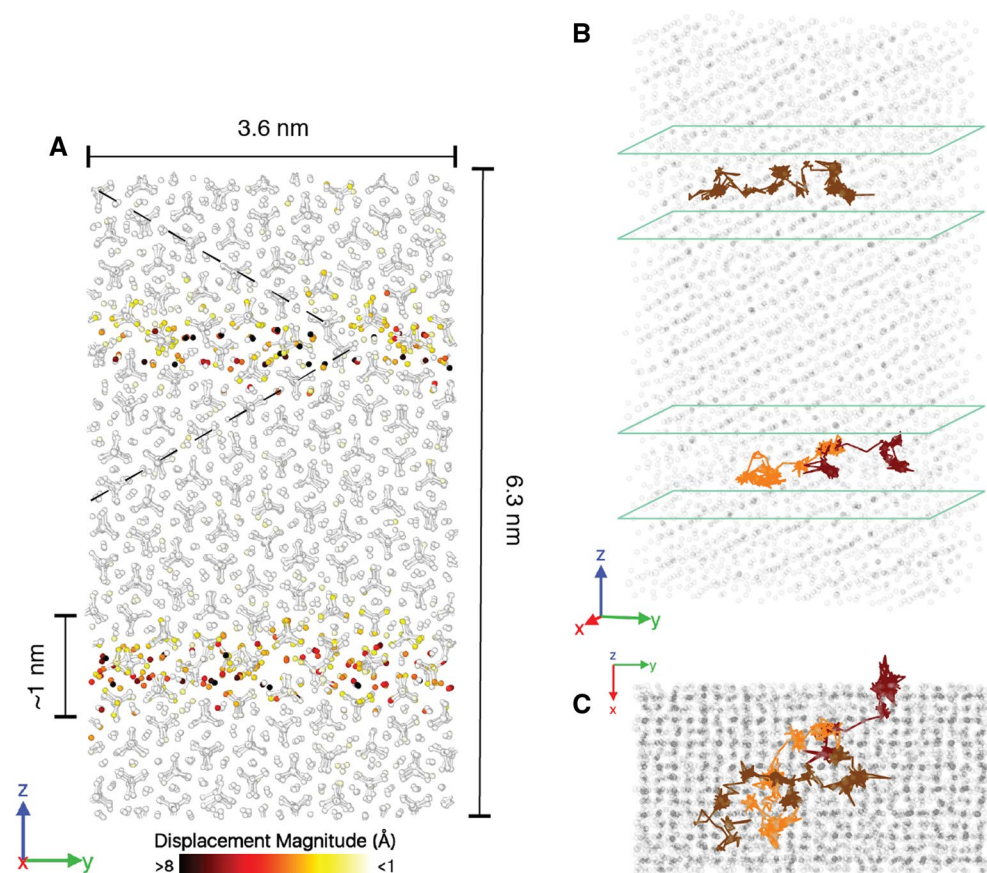
approximately 1.2–2 nm, and propagate cylindrical through the grain boundary interface, parallel to the a-axis of the two forsterite crystals (the *x*-axis in Fig. 4, the dashed green line outlines such a diffusion channel). When analysing exemplary trajectories of Mg atoms through these diffusion channels, one can observe a typical diffusion pattern where
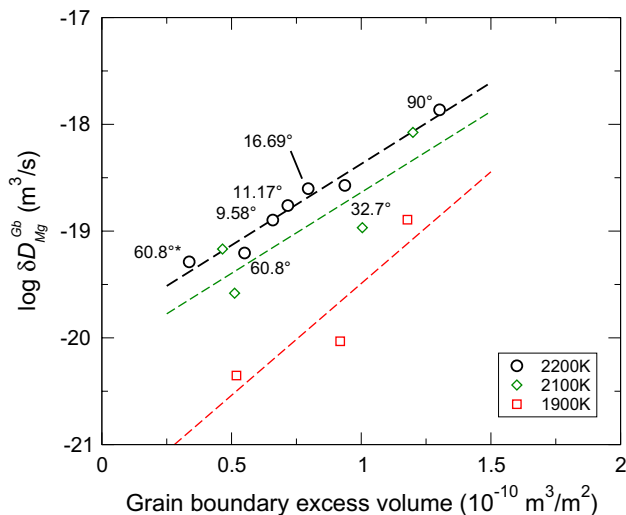
Fig. 6 Grain boundary diffusion coefficients (Mg) versus grain boundary excess volume for different *T. Dashed lines* are linear fits to the data. *Asterisks*-asymmetrical grain boundary

longer jumps are intermitted by phases of stagnation (e.g. Fig. 4 lower two panels). However, diffusion paths are not straight along the length of the channel but may also span its width entirely. High-angle grain boundaries on the other hand show no such diffusion channels (Fig. 5). Here, the area of highest mobility spans the entire grain boundary interface, about 1–2 nm in width. Atoms move more or less randomly in any direction parallel to the interfacial plane, whereas in the low-angle grain boundary, a long-term transport between two channels within the same GB interface plane (parallel to the *y*-axis in Fig. 4) should be considered rather slow, thus greatly limiting diffusion in this direction.

These two modes of transport, however, do not necessarily result in enhanced or reduced overall self-diffusion within a GB. Instead, it seems that the rate-determining factor is the overall excess volume of a grain boundary at any given temperature. Figure 6 shows the calculated grain boundary diffusion coefficients as a function of excess volume for different temperatures. Both slowest and fastest diffusions are observed in high-angle grain boundaries (60.80° and 90° misorientation). On the other hand, the relation to the grain boundary energy is much less pronounced, as e.g. the 32.70° GB exhibits the overall lowest GB energy (at ambient conditions) of the set investigated by Adjaoud et al. (2012). A theoretical relationship between excess volume and self-diffusion coefficients has previously been proposed by Chuvil'deev (1996). More generalised, excess volume as a measure of 'non-equilibrium state' of GBs in metals has been suggested to correlate with key physical properties such as sliding, migration, and segregation (Chuvil'deev et al. 2002; Petegem et al. 2003). Tucker

and McDowell (2011) infer from atomistic simulations that different initial GB configurations retain their excess volume differently under stress. This raises the question of how the self-diffusion coefficients presented here will vary with the respective GB excess volume under pressure (e.g. under mantle conditions). It is likely that different forsterite GB configurations will react differently to higher pressures and thus change in their relative contribution to average diffusion in the polycrystalline bulk rock. In real forsterite aggregates, the predominant grain boundary angles range from 60° to 90° while low-angle grain boundaries play a minor role (Marquardt et al. 2015). This suggests that when comparing the MD results to bulk diffusion rates in such aggregates, a weighted average of the diffusion coefficients of the high-angle grain boundaries seems a sensible choice. This also suggest that during mantle deformation, the bulk diffusion rates (and mechanism) will change depending on a preferred orientation that may be developed, i.e. when certain misorientation angles begin to dominate as opposed to a random distribution.

In the literature of grain boundary diffusion, the effective grain boundary width is defined as the region of increased atomic mobility (White 1973). Given that the grain boundaries of our MD study are so different, it is not easy to derive this quantity unambiguously for the different misorientations. Based on our visual inspection (Figs. 4, 5), the effective grain boundary width is consistent with previous estimates of one to two nanometres. Recently, Sun et al. (2016) systematically investigated the structure of the presented 60.8° misorientation grain boundary in terms of atomic distortions. Among others, they derived a three-dimensional continuum model for atomic displacement, distortion, and disclination density fields. Depending on the element and property, the structural grain boundary width appears to be broader or narrower, ultimately leading to an effective structural GB width similar to the effective GB width of diffusion.

Conclusion

From the preceding discussion, we may draw the following conclusions: (1) the grain boundary diffusivity in olivine depends explicitly on the type of GB, specifically on its excess volume, (2) (self-) diffusion in low-angle grain boundaries shows a strong anisotropy which may be explained by their structure of stacked (partial) dislocations. On the contrary, the GB diffusion in high-angle GB is essentially isotropic in the GB plane, and (3) classical MD simulations are a viable tool to study diffusive processes at within grain boundaries at high temperatures, given that sufficiently long trajectories can be achieved.

Further work should be focused on the effect of pressure on the excess volume and the related self-diffusion in forsterite grain boundaries in order to obtain a better understanding of GB diffusion in olivine under conditions of the upper mantle.

References

Adjaoud O, Steinle-Neumann G, Jahn S (2008) Mg_2SiO_4 liquid under high pressure from molecular dynamics. Chem Geol 256:185–192. doi:10.1016/j.chemgeo.2008.06.031

Adjaoud O, Steinle-Neumann G, Jahn S (2011) Transport properties of Mg_2SiO_4 liquid at high pressure: physical state of a magma ocean. Earth Planet Sci Lett 312:463–470. doi:10.1016/j.epsl.2011.10.025

Adjaoud O, Marquardt K, Jahn S (2012) Atomic structures and energies of grain boundaries in Mg_2SiO_4 forsterite from atomistic modeling. Phys Chem Miner 39:749–760. doi:10.1007/s00269-012-0529-5

Allen MP, Tildesley DJ (1989) Computer simulation of liquids. Clarendon Press, New York

Ammann MW, Brodholt JP, Dobson DP (2010) Simulating diffusion. Rev Miner Geochem 71(1):201–224. doi:10.2138/rmg.2010.71.10

Chakraborty S, Farver JR, Yund RA, Rubie DC (1994) Mg tracer diffusion in synthetic forsterite and San Carlos olivine as a function of P, T and fO_2. Phys Chem Miner 21(8):489–500. doi:10.1007/BF00203923

Chuvil'deev VN (1996) Micromechanism of deformation-stimulated grain-boundary self-diffusion: I. Effect of excess free volume on the free energy and diffusion parameters of grain boundaries. Phys Met Metallogr 81:463–468

Chuvil'deev VN, Kopylov VI, Zeiger W (2002) A theory of non-equilibrium grain boundaries and its applications to nano- and microcrystalline materials processed by ECAP. Ann Chim Sci Mater 27(3):55–64

Condit RH, Weed HC, Piwinskii AJ (1985) A technique for observing oxygen diffusion along grain boundary regions in synthetic forsterite. Am Geophys Union. doi:10.1029/GM031p0097

Dohmen R, Milke R (2010) Diffusion in polycrystalline materials: grain boundaries, mathematical models, and experimental data. Rev Miner Geochem 72(1):921–970. doi:10.2138/rmg.2010.72.21

Dohmen R, Chakraborty S, Becker HW (2002) Si and O diffusion in olivine and implications for characterizing plastic flow in the mantle. Geophys Res Lett 29(21):26–1–26–4. doi:10.1029/2002GL015480

Dohmen R, Becker HW, Chakraborty S (2007) Fe–Mg diffusion in olivine I: experimental determination between 700 and 1,200 °C as a function of composition, crystal orientation and oxygen fugacity. Phys Chem Miner 34(6):389–407. doi:10.1007/s00269-007-0157-7

Farber DL, Williams Q, Ryerson FJ (1994) Diffusion in Mg_2SiO_4 polymorphs and chemical heterogeneity in the mantle transition zone. Nature 371(6499):693–695. doi:10.1038/371693a0

Farver JR, Yund RA (2000) Silicon diffusion in forsterite aggregates: implications for diffusion accommodated creep. Geophys Res Lett 27(15):2337–2340. doi:10.1029/2000GL008492

Farver JR, Yund RA, Rubie DC (1994) Magnesium grain boundary diffusion in forsterite aggregates at 1000–1300 °C and 0.1 MPa to 10 GPa. J Geophys Res Solid 99(B10):19,809–19,819. doi:10.1029/94JB01250

Fei H, Hegoda C, Yamazaki D, Wiedenbeck M, Yurimoto H, Shcheka S, Katsura T (2012) High silicon self-diffusion coefficient in dry forsterite. Earth Planet Sci Lett 345348:95–103. doi:10.1016/j.epsl.2012.06.044

Fei H, Wiedenbeck M, Yamazaki D, Katsura T (2013) Small effect of water on upper-mantle rheology based on silicon self-diffusion coefficients. Nature 498(7453):213–215. doi:10.1038/nature12193

Fei H, Koizumi S, Sakamoto N, Hashiguchi M, Yurimoto H, Marquardt K, Miyajima N, Yamazaki D, Katsura T (2016) New constraints on upper mantle creep mechanism inferred from silicon grain-boundary diffusion rates. Earth Planet Sci Lett 433:350–359. doi:10.1016/j.epsl.2015.11.014

Finkelstein GJ, Dera PK, Jahn S, Oganov AR, Holl CM, Meng Y, Duffy TS (2014) Phase transitions and equation of state of forsterite to 90 GPa from single-crystal X-ray diffraction and molecular modeling. Am Mineral 99:35–43. doi:10.2138/am.2014.4526

Fisler DK, Mackwell SJ (1994) Kinetics of diffusion-controlled growth of fayalite. Phys Chem Miner 21(3):156–165. doi:10.1007/BF00203146

Gardés E, Wunder B, Marquardt K, Heinrich W (2012) The effect of water on intergranular mass transport: new insights from diffusion-controlled reaction rims in the MgO-SiO_2 system. Contrib Miner Pet 164(1):1–16. doi:10.1007/s00410-012-0721-0

Ghosh DB, Karki BB (2013) First principles simulations of the stability and structure of grain boundaries in Mg_2SiO_4 forsterite. Phys Chem Miner 41(3):163–171. doi:10.1007/s00269-013-0633-1

Gurmani SF, Jahn S, Brasse H, Schilling FR (2011) Atomic scale view on partially molten rocks: molecular dynamics simulations of melt-wetted olivine grain boundaries. J Geophys Res 116:B12,209. doi:10.1029/2011JB008519

Hansen LN, Zimmerman ME, Kohlstedt DL (2012) The influence of microstructure on deformation of olivine in the grain-boundary sliding regime. J Geophys Res Solid. doi:10.1029/2012JB009305

Hartmann K, Wirth R, Markl G (2008) P-T-X-controlled element transport through granulite-facies ternary feldspar from Lofoten, Norway. Contrib Miner Pet 156(3):359–375. doi:10.1007/s00410-008-0290-4

Hirth G, Kohlstedt D (2013) Rheology of the upper mantle and the mantle wedge: a view from the experimentalists. Am Geophys Union. doi:10.1029/138GM06

Hutter J, Iannuzzi M, Schiffmann F, VandeVondele J (2014) CP2K: atomistic simulations of condensed matter systems. Wiley Interdiscip Rev Comput Mol Sci 4(1):15–25. doi:10.1002/wcms.1159

Ikuhara Y, Nishimura H, Nakamura A, Matsunaga K, Yamamoto T, Lagerlf KPD (2003) Dislocation structures of low-angle and near-$\Sigma 3$ grain boundaries in alumina bicrystals. J Am Ceram Soc 86(4):595–602. doi:10.1111/j.1151-2916.2003.tb03346.x

Jahn S (2010) Integral modeling approach to study the phase behavior of complex solids: application to phase transitions in $MgSiO_3$ pyroxenes. Acta Crystallogr A 66:535–541. doi:10.1107/S0108767310026449

Jahn S, Madden PA (2007) Modeling Earth materials from crustal to lower mantle conditions: a transferable set of interaction potentials for the CMAS system. Phys Earth Planet Inter 162:129–139. doi:10.1016/j.pepi.2007.04.002

Jahn S, Madden PA (2008) Atomic dynamics of alumina melt: a molecular dynamics simulation study. Condens Matter Phys 11:169–178

Jahn S, Martoňák R (2008) Plastic deformation of orthoenstatite and the ortho- to high-pressure clinoenstatite transition: a metadynamics simulation study. Phys Chem Miner 35:17–23. doi:10.1007/s00269-007-0194-2

Karato S, Wu P (1993) Rheology of the upper mantle: a synthesis. Science 260(5109):771–778. doi:10.1126/science.260.5109.771

Keller LM, Wirth R, Rhede D, Kunze K, Abart R (2008) Asymmetrically zoned reaction rims: assessment of grain boundary diffusivities and growth rates related to natural diffusion-controlled mineral reactions. J Metamorph Geol 26(1):99–120. doi:10.1111/j.1525-1314.2007.00747.x

Kubo T, Shimojuku A, Ohtani E (2004) Mg–Fe interdiffusion rates in wadsleyite and the diffusivity jump at the 410-km discontinuity. Phys Chem Miner 31(7):456–464. doi:10.1007/s00269-004-0412-0

Madden PA, Heaton R, Aguado A, Jahn S (2006) From first-principles to material properties. J Mol Struct THEOCHEM 771:9–18. doi:10.1016/j.theochem.2006.03.015

Marquardt K, Petrishcheva E, Gardés E, Wirth R, Abart R, Heinrich AJ (2011) Grain boundary and volume diffusion experiments in yttrium aluminium garnet bicrystals at 1,723 K: a miniaturized study. Contrib Miner Pet 162:739–749. doi:10.1007/s00410-011-0622-7

Marquardt K, Rohrer GS, Morales L, Rybacki E, Marquardt H, Lin B (2015) The most frequent interfaces in olivine aggregates: the GBCD and its importance for grain boundary related processes. Contrib Miner Pet 170(4):1–17. doi:10.1007/s00410-015-1193-9

Martyna GJ, Tobias DJ, Klein ML (1994) Constant pressure molecular dynamics algorithms. J Chem Phys 101:4177–4189. doi:10.1063/1.467468

Nosé S, Klein ML (1983) Constant pressure molecular dynamics for molecular systems. Mol Phys 50:1055–1076. doi:10.1080/00268978300102851

Petegem SV, Torre FD, Segers D, Swygenhoven HV (2003) Free volume in nanostructured Ni. Scr Mater 48(1):17–22. doi:10.1016/S1359-6462(02)00322-6

Pommier A, Leinenweber K, Kohlstedt DL, Qi C, Garnero EJ, Mackwell SJ, Tyburczy JA (2015) Experimental constraints on the electrical anisotropy of the lithosphere–asthenosphere system. Nature 522(7555):202–206. doi:10.1038/nature14502

Ricoult DL, Kohlstedt DL (1983) Structural width of low-angle grain boundaries in olivine. Phys Chem Miner 9(3):133–138. doi:10.1007/BF00308370

Shimojuku A, Kubo T, Ohtani E, Yurimoto H (2004) Silicon self-diffusion in wadsleyite: implications for rheology of the mantle transition zone and subducting plates. Geophys Res Lett 31(13):L13,606. doi:10.1029/2004GL020002

Shimojuku A, Kubo T, Ohtani E, Nakamura T, Okazaki R, Dohmen R, Chakraborty S (2009) Si and O diffusion in $(Mg, Fe)_2SiO_4$ wadsleyite and ringwoodite and its implications for the rheology of the mantle transition zone. Earth Planet Sci Lett 284(12):103–112. doi:10.1016/j.epsl.2009.04.014

Stukowski A (2010) Visualization and analysis of atomistic simulation data with OVITO—the open visualization tool. Model Simul Mater Sci 18(1):015,012. doi:10.1088/0965-0393/18/1/015012

Sun X, Cordier P, Taupin V, Fressengeas C, Jahn S (2016) Continuous description of a grain boundary in forsterite from atomic scale simulations: the role of disclinations. Philos Mag 96(17):1757–1772. doi:10.1080/14786435.2016.1177232

Tucker GJ, McDowell DL (2011) Non-equilibrium grain boundary structure and inelastic deformation using atomistic simulations. Int J Plast 27(6):841–857. doi:10.1016/j.ijplas.2010.09.011

Watson EB (1986) An experimental study of oxygen transport in dry rocks and related kinetic phenomena. J Geophys Res Solid 91(B14):14,117–14,131. doi:10.1029/JB091iB14p14117

Watson GW, Oliver PM, Parker SC (1997) Computer simulation of the structure and stability of forsterite surfaces. Phys Chem Miner 25:70–78. doi:10.1007/s002690050088

White S (1973) Syntectonic recrystallization and texture development in quartz. Nature 244:276–278. doi:10.1038/244276a0